

# Do A or B Steps Have Faster Kinetics during Hexagonal Crystal Growth?

Guangxu Ju,<sup>1,\*</sup> Dongwei Xu,<sup>1,2</sup> Carol Thompson,<sup>3</sup> Matthew J. Highland,<sup>4</sup> Jeffrey A. Eastman,<sup>1</sup> Weronika Walkosz,<sup>5</sup> Peter Zapol,<sup>1</sup> and G. Brian Stephenson<sup>1,†</sup>

<sup>1</sup>Materials Science Division, Argonne National Laboratory, Argonne, IL 60439 USA

<sup>2</sup>School of Energy and Power Engineering, Huazhong University of Science and Technology, Wuhan, Hubei 430074, China

<sup>3</sup>Department of Physics, Northern Illinois University, DeKalb, IL 60115 USA

<sup>4</sup>X-ray Science Division, Argonne National Laboratory, Argonne, IL 60439 USA

<sup>5</sup>Department of Physics, Lake Forest College, Lake Forest, IL 60045 USA

(Dated: July 5, 2020)

The stacking sequence of hexagonal close-packed and related crystals typically results in steps on vicinal  $\{0001\}$  surfaces that have alternating  $A$  and  $B$  structures and growth behaviors. However, because it is difficult to experimentally identify which step is  $A$  or  $B$ , it has not been possible to determine which has faster adatom attachment kinetics. We show that surface X-ray scattering can unambiguously differentiate the growth behavior of  $A$  and  $B$  steps. Measurements performed *in situ* during growth of  $(0001)$  GaN find that the average width of terraces above  $A$  steps increases with growth rate, indicating that attachment rate constants are higher for  $A$  steps, in contrast to most predictions.

Our understanding of crystal growth is built on a powerful paradigm quantified by Burton, Cabrera, and Frank (BCF) [1-3], in which atoms are added to the growing crystal surface by attachment at the steps forming the edges of each exposed atomic layer, or terrace. The BCF model was originally developed for crystals with step heights of a full unit cell and step properties that are identical from step to step, for a given step direction. When the space group of the crystal includes screw axes or glide planes, the growth behavior on facets perpendicular to one of these symmetry elements can differ fundamentally [4]. In this case, the terraces can still all have the same atomic termination, but now have different in-plane orientations of their top layer. The fractional-unit-cell-height steps that separate these terraces have structures and properties that can vary from step to step, even for a fixed step direction.

A particularly subtle version of this effect occurs on the basal-plane  $\{0001\}$ -type surfaces of crystals having hexagonal close-packed (HCP) or related structures, which are normal to a  $6_3$  screw axis. Such crystals are made up of close-packed layers with 3-fold symmetry that alternate between opposite orientations, as shown by the  $\alpha$  and  $\beta$  terrace structures in Fig. 1(b). On a vicinal surface, the  $\alpha\beta\alpha\beta$  stacking sequence typically results in half-unit-cell-height steps. The lowest energy steps are normal to  $[01\bar{1}0]$ -type directions, and have alternating structures conventionally labelled  $A$  and  $B$  [5, 6] as shown in Fig. 1(a). When the in-plane azimuth of a step changes by  $60^\circ$ , e.g. from  $[01\bar{1}0]$  to  $[10\bar{1}0]$ , its structure changes from  $A$  to  $B$  or  $B$  to  $A$ .

The alternating nature of the steps on such surfaces has been imaged in several systems, including SiC [7], GaN [5, 8-12], AlN [13], and ZnO [14]. These systems typically show a tendency for local pairing of steps (i.e. alternating step spacings), and an “interlaced” structure in which the step pairs switch partners at corners where

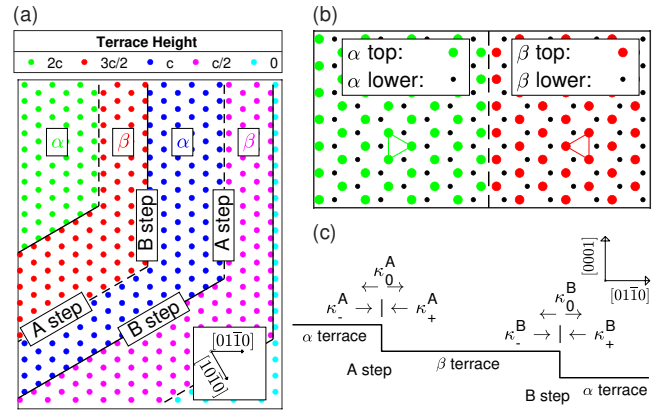


FIG. 1. Terrace and step structure of vicinal  $(0001)$  surface of an HCP-type crystal. (a) Circles show top-layer sites on each terrace, with color indicating height. Steps typically have lowest edge energy when they are normal to  $[01\bar{1}0]$ ,  $[10\bar{1}0]$ , or  $[1\bar{1}00]$ . Steps in a sequence have alternating structures,  $A$  and  $B$ . (b) Detail of  $\alpha$  and  $\beta$  terrace structures. Orientation of triangle of top-layer atoms around  $6_3$  screw axis shows difference between layers. (c) BCF theory kinetic coefficients for adatom attachment or transmission at each step.

their azimuth changes by  $60^\circ$ . These features are consistent with predictions that  $A$  and  $B$  steps have significantly different attachment kinetics [5, 10, 12, 15-20] that lead to unequal local fractions of  $\alpha$  and  $\beta$  terraces during growth. However, it has not been possible to experimentally distinguish the terrace orientation or step structure, and thus to determine whether  $A$  or  $B$  steps have faster kinetics.

Here we show that *in situ* surface X-ray scattering can distinguish the fraction of the surface covered by  $\alpha$  or  $\beta$  terraces during growth, unambiguously determining differences in the attachment kinetics at  $A$  and  $B$  steps. This is enabled by a high-quality single-crystal sample

and a micron-scale X-ray beam that illuminates a surface region with a uniform step azimuth. We demonstrate this for organo-metallic vapor phase epitaxy (OMVPE) of (0001) GaN, since the step properties of this surface have been a matter of some disagreement. A seminal study [5] of MBE growth of GaN observed alternating step shapes and proposed that the kinetic coefficients for adatom attachment are higher for  $A$  steps than  $B$  steps, i.e.  $A$  steps grow faster for a given supersaturation. The support for this highly cited prediction is based on an argument regarding the difference in dangling bonds between  $A$  and  $B$  steps, and an analogy with experimental results on GaAs (111) [21]. (Such face-centered cubic materials have  $A$  and  $B$  type steps that do not alternate between successive terraces and thus can be distinguished by their orientation [6].) However, subsequent theoretical studies of GaN (0001) OMVPE and MBE have consistently predicted that  $A$  steps have *smaller* adatom attachment coefficients than  $B$  steps. These have included kinetic Monte Carlo studies [15–18], arguments regarding dangling bonds [12], and *ab initio* calculations of kinetic barriers [19, 20]. Since these predictions rely on assumptions about the chemical states of adatoms, steps and terraces to build atomistic models of kinetic processes, there is a clear need for *in situ* measurements of the kinetics at  $A$  and  $B$  steps in relevant growth environments.

We present measurements of crystal truncation rods (CTRs) carried out *in situ* during OMVPE of (0001) GaN. CTRs are streaks of intensity extending in reciprocal space away from every Bragg peak in the direction normal to the crystal surface, which are sensitive to the surface structure [22]. We fit a model structure to these measurements to obtain the variation of the steady-state  $\alpha$  terrace fraction  $f_\alpha$  as a function of growth conditions, as well as the relaxation times of  $f_\alpha$  upon changing conditions. These results are compared to calculated dynamics based on a BCF model for a system with alternating step types, to quantify the differences in the attachment rates at  $A$  and  $B$  steps. Additional information on all these aspects is provided in a companion paper [23].

Figure 2 shows calculated intensity distributions along (01 $\bar{1}L$ ) and (10 $\bar{1}L$ ) CTRs for the GaN (0001) surface, demonstrating how their shapes vary with  $f_\alpha$ . Measurements discussed below indicate that the GaN surface under OMVPE conditions has a 3H(T1) reconstruction, in which 3 of every 4 Ga atoms in top-layer sites shown in Fig. 1 is bonded to an adsorbed hydrogen. The calculations in Fig. 2 include the effect of this reconstruction using relaxed atomic coordinates that have been calculated previously [24]. For  $f_\alpha = 0$  and  $f_\alpha = 1$ , there are alternating stronger and weaker intensities between the Bragg peaks, with the alternation being opposite for (01 $\bar{1}L$ ) and (10 $\bar{1}L$ ). For  $f_\alpha = 0.5$ , the intensities between the Bragg peaks are about the same, and there is no difference between the (01 $\bar{1}L$ ) and (10 $\bar{1}L$ ) CTRs. As required by symmetry, the (01 $\bar{1}L$ ) CTRs with  $f_\alpha = X$

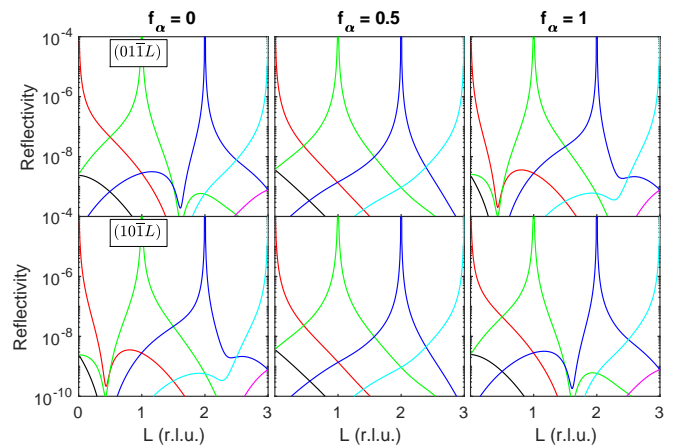


FIG. 2. Calculated CTR intensities for a vicinal surface with the 3H(T1) reconstruction. Top and bottom rows show the families of CTRs along (01 $\bar{1}L$ ) and (10 $\bar{1}L$ ), respectively. Black, red, green, blue, cyan, and magenta curves are for CTRs from the  $L_0 = -1$  to 4 Bragg peaks, respectively. Values of  $f_\alpha$  for each column are given at the top.

are identical to the (10 $\bar{1}L$ ) CTRs with  $f_\alpha = 1 - X$ , for any value  $X$ . The same qualitative behavior is obtained for alternative surface reconstructions [23].

We performed *in situ* measurements of the CTRs in the OMVPE environment at the Advanced Photon Source beamline 12ID-D [25]. At an incidence angle of  $2^\circ$ , the  $10 \mu\text{m}$  X-ray beam illuminated an area of  $10 \times 300 \mu\text{m}$ . To obtain sufficient signal, we used a wide-bandwidth “pink” beam setup [26, 27]. Two types of measurements were performed. We determined the steady-state terrace fractions  $f_\alpha^{ss}$  under four different growth/evaporation conditions by scanning the detector along the (01 $\bar{1}L$ ) and (10 $\bar{1}L$ ) CTRs while continuously maintaining steady-state growth or evaporation. We also observed the dynamics of  $f_\alpha$  after an abrupt change in conditions.

The four conditions studied are summarized in Table I. Deposition is transport limited, with the deposition rate proportional to the supply of the Ga precursor (triethylgallium, TEGa), with a large excess of the N precursor ( $\text{NH}_3$ ) constantly supplied. We investigated conditions of zero deposition (no supply of TEGa) as well as a TEGa supply of  $0.033 \mu\text{mole}/\text{min}$ . For both of these deposition rates, we used two carrier gas compositions: 50%  $\text{H}_2 + 50\%$   $\text{N}_2$ , and 0%  $\text{H}_2 + 100\%$   $\text{N}_2$ . The addition of  $\text{H}_2$  to the carrier gas enhances evaporation of GaN, so that the net growth rate (deposition rate minus evaporation rate) is slightly lower; at zero deposition rate, the net growth rate is negative. The net growth rates  $G$  determined for all four conditions [23] are given in Table I. The substrate temperature was  $1077 \pm 5 \text{ K}$  for all four conditions. The substrate used was a GaN single crystal [28] with an offset of  $0.52^\circ$  from (0001) on an azimuth  $5^\circ$  from [01 $\bar{1}0$ ] towards [10 $\bar{1}0$ ]. With this low-dislocation-density substrate and at these low growth rates, the pre-

TABLE I. Values of terrace fraction  $f_\alpha^{ss}$  obtained from fits to CTR intensities measured under 4 growth conditions.

Growth condition index	TEGa flow ( $\mu\text{mole}/\text{min}$ )	H <sub>2</sub> frac. in carrier	Net growth rate $G$ (ML/s)	Terrace fraction $f_\alpha^{ss}$
1	0.000	50%	-0.0018	$0.111 \pm 0.013$
2	0.000	0%	0.0000	$0.461 \pm 0.018$
3	0.033	50%	0.0109	$0.811 \pm 0.014$
4	0.033	0%	0.0127	$0.868 \pm 0.011$

viously reported instability to step bunching [29] was not observed.

Figure 3 shows the measured steady-state CTR intensities as a function of  $L$ , for both the  $(01\bar{1}L)$  and  $(10\bar{1}L)$  CTRs and at all four conditions. The qualitative behavior agrees with that expected from a variation in  $f_\alpha$  shown in Fig. 2, with alternating higher and lower intensities between the Bragg peaks under some conditions, and opposite behavior of the two CTRs. To obtain values of the steady-state terrace fraction  $f_\alpha^{ss}$  for each of the four conditions, we fit calculated CTR intensities to the measured profiles. For each condition, both the  $(01\bar{1}L)$  and  $(10\bar{1}L)$  CTRs were simultaneously fit [23]. Fits are shown in Fig. 2, and values of  $f_\alpha^{ss}$  obtained are given in Table I. While the 3H(T1) reconstruction gives the best fit to all conditions, similar  $f_\alpha^{ss}$  values are obtained using alternative reconstructions [23].

The marked increase in  $f_\alpha$  as  $G$  is increased reveals the qualitative difference between the kinetics at  $A$  and  $B$  steps during OMVPE of GaN: adatom attachment coefficients for  $A$  steps are larger. Thus a surface with initially equal  $\alpha$  and  $\beta$  terrace fractions will evolve to one with a high  $f_\alpha$  during growth, because of the initially higher adatom attachment rate at the  $A$  steps. Likewise, the higher detachment rate at  $A$  steps during evaporation will give a low  $f_\alpha$ .

We also observed the dynamics of the change in  $f_\alpha$  by recording the intensity at a fixed detector position as a function of time before and after an abrupt change between conditions, as shown in Figure 4(a). We chose positions near  $L = 1.6$  where the X-ray reflectivity  $R$  changes almost monotonically with  $f_\alpha$ . It is thus straightforward to obtain  $f_\alpha(t)$  from the intensity evolution using the calculated  $R(f_\alpha)$  [23], as shown in Fig. 4(b). The characteristic relaxation times ( $1/e$  decay point) were  $2200 \pm 200$  s and  $340 \pm 30$  s for the transitions from conditions 1 to 2 and 2 to 4, respectively.

To quantitatively relate the behavior of the terrace fraction to the kinetic properties of  $A$  and  $B$  steps, we have developed a model [23] based on BCF theory. Such models have been used extensively to understand growth behavior such as the step-bunching instability [30], pairing of steps [31], and competitive adsorption [32], typically where all steps in a sequence are equivalent. In our

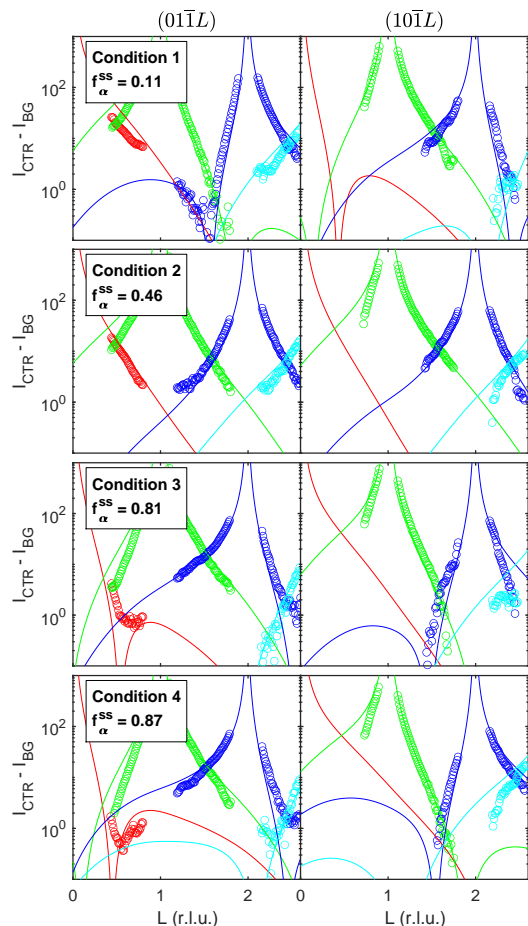


FIG. 3. Circles show measured net intensities of the  $(01\bar{1}L)$  CTRs and  $(10\bar{1}L)$  CTR families (left and right) for CTRs from the  $L_0 = 0, 1, 2, 3$  Bragg peaks, at each of four growth conditions. Curves show fits of both CTRs to obtain steady-state  $\alpha$  terrace fraction  $f_\alpha^{ss}$  at each condition.

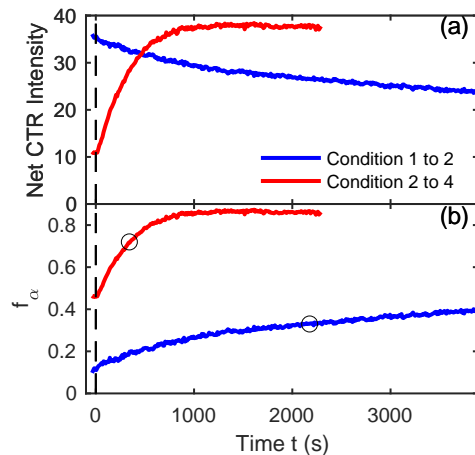


FIG. 4. Dynamics following a change of condition at  $t = 0$ . (a) Measured CTR intensities. (b) Calculated terrace fractions  $f_\alpha$ . Blue curves: condition 1 to 2 on the  $(10\bar{1}2)$  CTR at  $L = 1.627$ . Red curves: condition 2 to 4 on the  $(01\bar{1}2)$  CTR at  $L = 1.603$ . Circles show  $1/e$  relaxation times  $2200 \pm 200$  s and  $340 \pm 30$  s.

model, we consider an alternating sequence of two types of terraces,  $\alpha$  and  $\beta$ , and two types of steps,  $A$  and  $B$ , with properties that can differ, as shown in Fig. 1(c). We include the effects of step transparency [33] (i.e. adatom transmission across steps) and step-step repulsion [2].

The rate of change in the adatom density per unit area  $\rho_i$  on terrace type  $i = \alpha$  or  $\beta$  is written as

$$\frac{\partial \rho_i}{\partial t} = D \nabla^2 \rho_i - \frac{\rho_i}{\tau} + F, \quad (1)$$

where  $D$  is the adatom diffusivity,  $\tau$  is the adatom lifetime before evaporation, and  $F$  is the deposition flux of adatoms per unit time and area. The four boundary conditions for the flux at the steps terminating each type of terrace can be written as

$$-D \nabla \rho_\alpha^+ = +\kappa_-^A (\rho_\alpha^+ - \rho_{eq}^A) + \kappa_0^A (\rho_\alpha^+ - \rho_\beta^-), \quad (2)$$

$$-D \nabla \rho_\alpha^- = -\kappa_+^B (\rho_\alpha^- - \rho_{eq}^B) - \kappa_0^B (\rho_\alpha^- - \rho_\beta^+), \quad (3)$$

$$-D \nabla \rho_\beta^+ = +\kappa_-^B (\rho_\beta^+ - \rho_{eq}^B) + \kappa_0^B (\rho_\beta^+ - \rho_\alpha^-), \quad (4)$$

$$-D \nabla \rho_\beta^- = -\kappa_+^A (\rho_\beta^- - \rho_{eq}^A) - \kappa_0^A (\rho_\beta^- - \rho_\alpha^+). \quad (5)$$

As shown in Fig. 1(c),  $\kappa_+^j$  and  $\kappa_-^j$  are the kinetic coefficients for adatom attachment at a step of type  $j = A$  or  $B$  from below or above, respectively, and  $\kappa_0^j$  is the kinetic coefficient for transmission across the step. The  $+$  or  $-$  superscripts on  $\rho_i$  and  $\nabla \rho_i$  indicate evaluation at the downhill or uphill terrace boundaries, respectively. We consider the overall vicinal angle of the surface to fix the sum  $w$  of the widths of  $\alpha$  and  $\beta$  terraces, which are thus  $f_\alpha w$  and  $(1 - f_\alpha)w$ . We also assume relations between the equilibrium adatom densities at the steps  $\rho_{eq}^j$  and the terrace widths that reflect an effective repulsion between the steps owing to entropic and strain effects [2],

$$\rho_{eq}^j = \rho_{eq}^0 \exp(\mu_j/kT), \quad (6)$$

where  $\rho_{eq}^0$  is the equilibrium adatom density at zero growth rate, and the step chemical potentials  $\mu_j$  are

$$\frac{\mu_A}{kT} = -\frac{\mu_B}{kT} = \mathbf{M}(f_\alpha) \equiv \left(\frac{\ell}{w}\right)^3 \left[ \left(\frac{1-f_\alpha^0}{1-f_\alpha}\right)^3 - \left(\frac{f_\alpha^0}{f_\alpha}\right)^3 \right], \quad (7)$$

where  $\ell$  is the step repulsion length and  $f_\alpha^0$  is the terrace fraction at zero growth rate.

To solve this model we develop a quasi-steady-state expression for the dynamics of the terrace fraction  $f_\alpha$ . Under fairly general assumptions [23], the behavior of  $f_\alpha$  can be written as a function of the net growth rate,

$$G = \frac{F - \rho_{eq}^0/\tau}{\rho_0}. \quad (8)$$

This is simply the difference between the deposition  $F$  and a uniform evaporation  $\rho_{eq}^0/\tau$ , converted to ML/s using the site density  $\rho_0$ . The rate of change in  $f_\alpha$  is

$$\frac{df_\alpha}{dt} = \mathbf{K}^{dyn}(f_\alpha) \left( \frac{G}{\mathbf{K}^{ss}(f_\alpha)} - \frac{4\mathbf{M}(f_\alpha)\rho_{eq}^0}{w\rho_0} \right), \quad (9)$$

TABLE II. Parameter values obtained from the fit shown in Fig. 5, using  $w = 5.7 \times 10^{-8}$  m,  $\rho_0 = 1.13 \times 10^{19}$  m $^{-2}$  corresponding to the experiments. In this limit  $\kappa_+^A \gg \kappa_-^A$ , while  $\kappa_-^A$ ,  $\kappa_-^B$ , and  $\kappa_0^A$  approach zero.

Parameter	Value	Units
$D/\kappa_+^B$	$1.9 \times 10^{-8}$	(m)
$D/\kappa_0^B$	$1.1 \times 10^{-8}$	(m)
$D\rho_{eq}^0\ell^3$	$3.3 \times 10^{-23}$	(m $^3$ /s)
$f_\alpha^0$	0.44	-

where we have introduced the combined kinetic coefficient functions  $\mathbf{K}^{ss}(f_\alpha)$  and  $\mathbf{K}^{dyn}(f_\alpha)$ , which in the general case depend on all six  $\kappa_x^j$  coefficients [23].

The full steady state  $df_\alpha/dt = 0$  is obtained at a growth rate of

$$G^{ss}(f_\alpha) = \frac{4\mathbf{K}^{ss}(f_\alpha)\mathbf{M}(f_\alpha)\rho_{eq}^0}{w\rho_0}. \quad (10)$$

This equation for  $G^{ss}(f_\alpha)$  can be inverted to obtain the steady-state value  $f_\alpha^{ss}$  as a function of  $G$ .

We performed fits to the measured quantities (four  $f_\alpha^{ss}$  and two relaxation times) using the general expressions for  $\mathbf{K}^{ss}(f_\alpha)$  and  $\mathbf{K}^{dyn}(f_\alpha)$  [23]. The best fit, shown in Fig. 5, was obtained in the limit in which the  $\kappa_+^A$  coefficient is large, while the  $\kappa_-^A$ ,  $\kappa_-^B$ , and  $\kappa_0^A$  coefficients approach zero. In this case  $\mathbf{K}^{ss}(f_\alpha)$  and  $\mathbf{K}^{dyn}(f_\alpha)$  can be written as [23]

$$\mathbf{K}^{ss}(f_\alpha) = \left[ \frac{1}{\kappa_+^B} + \frac{(1-2f_\alpha)}{\kappa_0^B} - \frac{wf_\alpha(1-f_\alpha)}{D} \right]^{-1}, \quad (11)$$

$$\mathbf{K}^{dyn}(f_\alpha) = \left[ \frac{1}{\kappa_+^B} + \frac{1}{\kappa_0^B} + \frac{w(1-f_\alpha)}{D} \right]^{-1}. \quad (12)$$

We can fit the measurements directly using these expressions to obtain the four parameters given in Table II. Using estimates of  $D \approx 1.4 \times 10^{-7}$  m $^2$ /s and  $\rho_{eq}^0 \approx 3.4 \times 10^{11}$  m $^{-2}$  [23], these parameters imply kinetic coefficients of  $\kappa_+^B \approx 7.4$  m/s and  $\kappa_0^B \approx 13$  m/s, and a step repulsion length of  $\ell \approx 9 \times 10^{-10}$  m.

Our primary result, the positive slope of  $f_\alpha^{ss}(G)$ , determines the basic nature of the adatom attachment kinetics at  $A$  and  $B$  steps for GaN (0001) OMVPE. In general, this positive slope implies that  $A$  steps have faster kinetics than  $B$  steps, i.e. the attachment coefficients  $\kappa_x^A$  are larger than the  $\kappa_x^B$ . While a similar general shape of  $f_\alpha^{ss}(G)$  is produced by many combinations of the parameters in the BCF model that have faster  $A$  than  $B$  step kinetics, the best fit to our measurements is obtained in the specific limit of Eqs. (11,12). In this limit the  $A$  step has much faster attachment kinetics than the  $B$  step, with  $\kappa_+^A \gg \kappa_+^B$ . This limit also indicates that both  $A$  and  $B$  steps have standard positive Ehrlich-Schwoebel barriers, with adatom attachment from below significantly faster



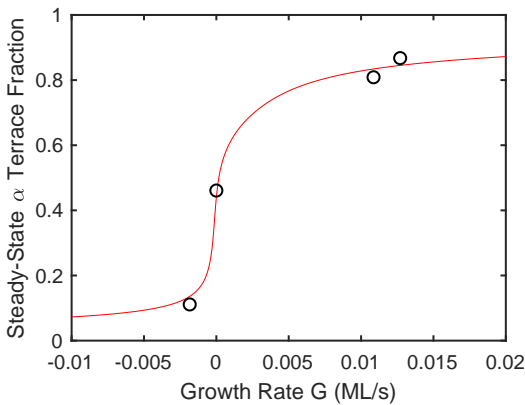


FIG. 5. Comparison of best-fit BCF model calculation to experimental points  $f_{\alpha}^{ss}$  vs.  $G$ . Also fit simultaneously with these four points were the two relaxation times given in Fig. 4.

than from above for the same supersaturation, and that the  $A$  step is non-transparent. We find that  $f_{\alpha}^0$  differs only slightly from the symmetrical value of  $1/2$ .

Our conclusion that  $A$  steps on GaN (0001) have higher attachment coefficients than  $B$  steps agrees with the original prediction [5], and motivates further theory development beyond [12, 15–20], in which various assumptions lead to the opposite conclusion. Both the predicted and observed step behavior can depend upon the chemical environment (e.g. OMVPE vs. MBE) and how it passivates the step edges. For example, a study of AlN OMVPE [13] found that  $f_{\alpha}$  apparently varies when large changes are made in the V/III ratio. It will be of interest in future theoretical work to consider GaN (0001) in the OMVPE environment with the 3H(T1) reconstruction.

These measurements demonstrate that microbeam X-ray scattering from surfaces with well-defined step azimuths can distinguish the fraction of  $\alpha$  and  $\beta$  terraces. *In situ* measurements of this type during growth can thus unambiguously differentiate the growth behavior of  $A$  and  $B$  steps on basal plane surfaces of any HCP-type crystal. These include not only important compound semiconductors, but also a third of the crystalline elements and numerous more complex systems.

Work supported by the U.S Department of Energy (DOE), Office of Science, Office of Basic Energy Sciences, Materials Science and Engineering Division. Experiments performed at the Advanced Photon Source beamline 12ID-D, a DOE Office of Science user facility.

\* correspondence to: [juguangxu@gmail.com](mailto:juguangxu@gmail.com); current address: Lumileds Lighting Co., San Jose, CA 95131 USA.

† correspondence to: [stephenson@anl.gov](mailto:stephenson@anl.gov)

[1] W. Burton, N. Cabrera, and F. Frank, The growth of crystals and the equilibrium structure of their surfaces,

- Philos. Trans. Royal. Soc. London Ser. A* **243**, 299 (1951).
- [2] H.-C. Jeong and E. D. Williams, Steps on surfaces: experiment and theory, *Surf. Sci. Rep.* **34**, 171 (1999).
- [3] D. P. Woodruff, How does your crystal grow? a commentary on Burton, Cabrera and Frank (1951) ‘The growth of crystals and the equilibrium structure of their surfaces’, *Phil. Trans. R. Soc. A.* **373**, 20140230 (2015).
- [4] W. J. P. van Enkevort and P. Bennema, Interlacing of growth steps on crystal surfaces as a consequence of crystallographic symmetry, *Acta Crystallogr. Sec. A* **60**, 532 (2004).
- [5] M. H. Xie, S. M. Seutter, W. K. Zhu, L. X. Zheng, H. Wu, and S. Y. Tong, Anisotropic step-flow growth and island growth of GaN(0001) by molecular beam epitaxy, *Phys. Rev. Lett.* **82**, 2749 (1999).
- [6] M. Giesen, Step and island dynamics at solid/vacuum and solid/liquid interfaces, *Prog. Surf. Sci.* **68**, 1 (2001).
- [7] A. R. Verma, CI. Observations on carborundum of growth spirals originating from screw dislocations, *Philos. Mag.* **42**, 1005 (1951).
- [8] B. Heying, E. J. Tarsa, C. R. Elsass, P. Fini, S. P. DenBaars, and J. S. Speck, Dislocation mediated surface morphology of GaN, *J. Appl. Phys.* **85**, 6470 (1999).
- [9] S. S. Vézian, J. Massies, F. Semond, and N. Grandjean, Surface morphology of GaN grown by molecular beam epitaxy, *Mater. Sci. Eng. B* **82**, 56 (2001).
- [10] M. H. Xie, M. Gong, E. K. Y. Pang, H. S. Wu, and S. Y. Tong, Origin of triangular island shape and double-step bunching during GaN growth by molecular-beam epitaxy under excess Ga conditions, *Phys. Rev. B* **74**, 085314 (2006).
- [11] H. Zheng, M. H. Xie, H. S. Wu, and Q. K. Xue, Kinetic energy barriers on the GaN(0001) surface: A nucleation study by scanning tunneling microscopy, *Phys. Rev. B* **77**, 045303 (2008).
- [12] H. Turski, M. Siekacz, Z. R. Wasilewski, M. Sawicka, S. Porowski, and C. Skierbiszewski, Nonequivalent atomic step edges - role of gallium and nitrogen atoms in the growth of InGaIn layers, *J. Cryst. Growth* **367**, 115 (2013).
- [13] M. Pristovsek, K. Bellman, F. Mehnke, J. Stellmach, T. Wernicke, and M. Kneissl, Surface reconstructions of (0001) AlN during metal-organic vapor phase epitaxy, *Phys. Status Solidi B* **254**, 1600711 (2017).
- [14] Y. Chen, H.-J. Ko, S.-K. Hong, T. Yao, and Y. Segawa, Morphology evolution of ZnO(0001) surface during plasma-assisted molecular-beam epitaxy, *Appl. Phys. Lett.* **80**, 1358 (2002).
- [15] M. A. Załuska-Kotur, F. Krzyżewski, and S. Krukowski, Surface patterns due to step flow anisotropy formed in crystal growth process, *J. Non-Cryst. Solids* **356**, 1935 (2010).
- [16] M. A. Załuska-Kotur, F. Krzyżewski, and S. Krukowski, Double step structure and meandering due to the many body interaction at GaN(0001) surface in N-rich conditions, *J. Appl. Phys.* **109**, 023515 (2011).
- [17] M. Chugh and M. Ranganathan, Lattice kinetic monte carlo simulation study of the early stages of epitaxial GaN(0001) growth, *Appl. Surf. Sci.* **422**, 1120 (2017).
- [18] D. Xu, P. Zapol, G. B. Stephenson, and C. Thompson, Kinetic monte carlo simulations of GaN homoepitaxy on c- and m-plane surfaces, *J. Chem. Phys.* **146**, 144702 (2017).
- [19] T. Akiyama, T. Ohka, K. Nakamura, and T. Ito,

- Ab initio study for adsorption and desorption behavior at step edges of GaN(0001) surface, *J. Cryst. Growth* **532**, 125410 (2020).
- [20] T. Akiyama, T. Ohka, K. Nakamura, and T. Ito, Ab initio study for adsorption and desorption behavior at step edges of AlN(0001) and GaN(0001) surfaces, *Jpn. J. Appl. Phys.* **59**, SGGK03 (2020).
- [21] A. R. Avery, H. T. Dobbs, D. M. Holmes, B. A. Joyce, and D. D. Vvedensky, Nucleation and growth of islands on GaAs surfaces, *Phys. Rev. Lett.* **79**, 3938 (1997).
- [22] I. K. Robinson, Crystal truncation rods and surface roughness, *Phys. Rev. B* **33**, 3830 (1986).
- [23] G. Ju, D. Xu, C. Thompson, M. J. Highland, J. A. Eastman, W. Walkosz, P. Zapol, and G. B. Stephenson, Dynamics of atomic steps on GaN (0001) during vapor phase epitaxy (2020), placeholder for the reference to accompanying PRB.
- [24] W. Walkosz, P. Zapol, and G. B. Stephenson, Metallicity of InN and GaN surfaces exposed to NH<sub>3</sub>, *Phys. Rev. B* **85**, 033308 (2012).
- [25] G. Ju, M. J. Highland, A. Yanguas-Gil, C. Thompson, J. A. Eastman, H. Zhou, S. M. Brennan, G. B. Stephenson, and P. H. Fuoss, An instrument for in situ coherent x-ray studies of metal-organic vapor phase epitaxy of III-nitrides, *Rev. Sci. Instrum.* **88**, 035113 (2017).
- [26] G. Ju, M. J. Highland, C. Thompson, J. A. Eastman, P. H. Fuoss, H. Zhou, R. Dejus, and G. B. Stephenson, Characterization of the x-ray coherence properties of an undulator beamline at the Advanced Photon Source, *J. of Synchrotron Radiat.* **25**, 1036 (2018).
- [27] G. Ju, D. Xu, M. J. Highland, C. Thompson, H. Zhou, J. A. Eastman, P. H. Fuoss, P. Zapol, H. Kim, and G. B. Stephenson, Coherent x-ray spectroscopy reveals the persistence of island arrangements during layer-by-layer growth, *Nat. Phys.* **15**, 589 (2019).
- [28] GANKIBAN<sup>TM</sup> from SixPoint Materials, Inc., [spmaterials.com](http://spmaterials.com).
- [29] M. V. R. Murty, P. Fini, G. B. Stephenson, C. Thompson, J. A. Eastman, A. Munkholm, O. Auciello, R. Jothilingam, S. P. DenBaars, and J. S. Speck, Step bunching on the vicinal GaN (0001) surface, *Phys. Rev. B* **62**, R10661 (2000).
- [30] L. Guin, M. E. Jabbour, L. Shaabani-Ardali, L. Benoit-Maréchal, and N. Triantafyllidis, Stability of vicinal surfaces: Beyond the quasistatic approximation, *Phys. Rev. Lett.* **124**, 036101 (2020).
- [31] O. Pierre-Louis and J.-J. Métois, Kinetic step pairing, *Phys. Rev. Lett.* **93**, 165901 (2004).
- [32] T. Hanada, Thermodynamic model for metal-organic vapor-phase epitaxy of N-polar group-III nitrides in step-flow growth mode: Hydrogen, competitive adsorption, and configuration entropy, *Phys. Rev. Materials* **3**, 103404 (2019).
- [33] O. Pierre-Louis, Phase field models for step flow, *Phys. Rev. E* **68**, 021604 (2003).